JSR Publications

Available Online

J. Sci. Res. **12** (4), 499-515 (2020)

JOURNAL OF SCIENTIFIC RESEARCH

www.banglajol.info/index.php/JSR

Effect of Al_2O_3 Nanoparticles and Cylindrical Pins on Natural Convection Heat Transfer in a C-Shaped Enclosure

M. Y. Arafat*, F. Faisal

Department of Mechanical Engineering, Bangladesh University of Engineering and Technology, Dhaka-1000, Bangladesh

Received 26 February 2020, accepted in final revised form 31 May 2020

Abstract

A numerical study has been conducted to investigate the transport mechanism of natural convection in a C-shaped enclosure filled with water-Al_2O_3 nanofluid for various pertinent parameters. The effects of the volume fraction of the Al_2O_3 nanoparticles, Rayleigh number, and radius of inserted cylindrical pins on the temperature, velocity, heat flux profiles and average Nusselt number have been investigated. General correlations for the effective thermal conductivity and viscosity of nanofluids are used for this analysis. The governing mass, momentum and energy equations are solved numerically with the finite volume method using the SIMPLER algorithm. The results show that addition of nanoparticle improves the heat transfer performance. Insertion of cylindrical pins of lower radius increases the average Nusselt number irrespective of Rayleigh number. But anomaly has been observed while pins of higher radius are inserted due to enormous disturbance in the fluid.

Keywords: Natural convection; C-Shaped enclosure; Nanofluid; Cylindrical pins; Finite volume method.

doi: http://dx.doi.org/10.3329/jsr.v12i4.45605 J. Sci. Res. **12** (4), 499-515 (2020)

1. Introduction

Natural convection heat transfer plays a preeminent role in the engineering domain for its unique but immense applications in electronic cooling, heat exchangers, double pane windows and so on [1]. Enhancing the heat transfer performance and effectiveness in these systems is a crucial issue from the energy saving as well as cost minimization contexts which are severely hindered by the ineffectual thermal conduction of conventional heat transfer fluids. An innovative and new technique to boost up heat transfer is dispersion of nano sized solid particles into the base fluid (i.e., nanofluid). Due to the tiny sizes and increased specific surface areas of the nanoparticles, nanofluid may

*Corresponding author: yeashir.arafat45@gmail.com

achieve improved properties like better thermal conductivity, high level of stability, lower tendency in flow passages blocking and so forth.

In the past decade, several researchers have investigated natural convection in enclosures with various shapes, nanofluids and thermal boundary conditions [2-6]. Oztop and Abu-nada [7] studied numerically free convection of nanofluid in partially heated rectangular cavities and observed boosting of the heat transfer rate upon increment in nanoparticles volume fraction as well as height of heater. In another numerical simulation, Abu-nada and Oztop [8] observed the effect of inclination angle on free convection in a square cavity containing Cu-water nanofluid. They observed that Rayleigh numbers being lowered, the effect of varying inclination angle on the rate of heat transfer became insignificant. Abu-nada *et al*. [9] numerically investigated that at high Rayleigh numbers, though the heat transfer rate was sensitive to viscosity model, the thermal conductivity model did not affect the heat transfer rate. Ögüt [10] analytically examined free convection heat transfer of water-based nanofluids in an inclined square cavity with a heater of constant heat flux positioned at the mid-point of its left wall and observed escalation of heat transfer rate at higher Rayleigh number and increased nanoparticles content.

Ghasemi and Aminossadati [11] studied the influence of Brownian movement of nanoparticles on natural convection of CuO-water nanofluid enclosed in a right triangular cavity and found that while considering Brownian movement, the heat transfer rate was significantly influenced by the volume fraction of nanoparticles, the aspect ratio of cavity, location of the heat source as well as variation of Rayleigh numbers. Sheikhzadeh *et al.* [12] carried out a numerical analysis on free convection of the TiO_2-water nanofluid within rectangular enclosures heated differentially on adjacent walls and concluded that increasing both the Rayleigh number and volume fraction resulted in enhancement of average Nusselt number. Mahmoodi [13] investigated numerically free convection in L-shaped enclosure using Cu-water nanofluid. The obtained results show that at all Rayleigh numbers considered, the average Nusselt number enhanced upon raising the aspect ratio of enclosure and nanoparticles content.

Natural convection heat transfer in a C-shaped enclosure having Cu-water nanofluid had been studied as well by Mahmoodi and Hashemi [14] to analyze the effect of variable aspect ratio of cavity, Rayleigh number and volume fraction of the nanoparticles on average Nusselt number. Mansour *et al.* [15] numerically examined the effect of localized heat source on natural convection inside a C-shaped enclosure having Cu-water nanofluid. Makulati *et al.* [16] investigated the effect of magnetic field on natural convection heat transfer in an inclined C-shaped cavity containing alumina-water nanofluid and concluded that Hartmann number being increased, the influence of nanofluid on average Nusselt number was lessened. Chamkha *et al.* [17] numerically studied the natural heat transfer process in C-shaped cavity in presence of magnetic field and determined a threshold value of Hartman number for the most efficient heat transfer in that cavity. Mohebbi *et al*. [18] numerically explored the effect of heat source location along with varying Rayleigh

number, yielding most suitable Nusselt number for natural convection in a C-shaped enclosure.

Being chemically very stable and almost insoluble in water, acids, and bases Al_2O_3 nanoparticles have received a great attention in past few years [19]. Sheikholeslami *et al*. [20] simulated the effect of horizontal magnetic field on free convection heat transfer in a concentric annulus filled with Al_2O_3-water nanofluid to show that the enhancement in heat transfer is an increasing function of Hartmann number. Ahmed *et al.* [21] observed a high gradient in wall temperatures when the water is replaced by Al_2O_3-water nanofluid particularly at higher volume fraction. In an experiment concerning nanofluids, Sinha *et al.* [22] revealed a consistent rise in the heat transfer with increasing volumetric concentration of Al_2O_3 nanoparticles at any given Reynolds number. Sheremet *et al*. [23] studied the unsteady natural convection in an inclined square cavity filled with Al_2O_3-water nanofluid and found that temperature-varying wall affects the heat transfer as well as fluid flow with time. It was also observed that the shape of nanoparticles had a significant effect on natural convection heat transfer of Al_2O_3-water nanofluid [24,25].

The objective of this paper is to investigate numerically the transport mechanism of natural convection in a C-shaped enclosure filled with water-Al_2O_3 nanofluid. As the total heat flux distribution and consequences of cylindrical pin insertion in a C-shaped enclosure have not been studied yet, special attention has been paid to inspect the effects of the volume fraction of the nanoparticles, Rayleigh number and insertion of cylindrical pins on the temperature, velocity and heat flux profile in the enclosure for a fixed aspect ratio. Moreover, the impact of cylindrical pin radii on average Nusselt number has also been demonstrated.

2. Mathematical Modeling

A schematic view of the C-shaped enclosure considered in this study is shown in Fig. 1. The top, left and bottom walls of the enclosure are maintained at elevated temperature, whereas the inner horizontal and vertical walls are kept cold. The right most vertical walls are well insulated shown by dark lines. The height and the thickness of the enclosure are represented by H and W respectively. The aspect ratio of the enclosure is thus defined as AR = W/H. Since the length of the cavity is considered to be much longer compared to its height and thickness, the problem can be considered as two dimensional. The whole cavity is assumed to be replete with homogeneous Al_2O_3-water nanofluid. Thermal equilibrium and no slip conditions are taken into account for the nanoparticles and the base fluid. The constant thermo-physical properties of Al_2O_3 nanoparticles and water (base fluid) are adopted from Oztop *et al.* [26] and listed in Table 1. The nanofluid is considered to be incompressible and Newtonian while the nanofluid flow is assumed to be laminar. Density variation of the nanofluid follows Boussinesq approximation [27].

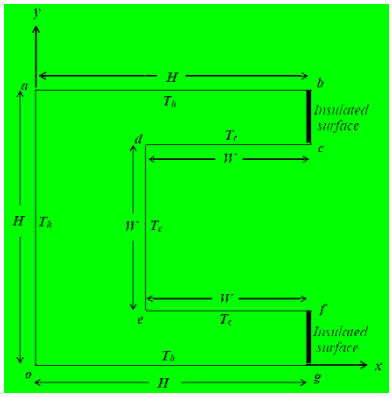

Fig. 1. Schematic diagram of the C-shaped enclosure under consideration.

Table 1. Thermo-physical properties of water and Al_2O_3 nanoparticles [26].

Physical properties	Water	Al_2O_3
C_p (J·kg^{-1}·k^{-1})	4179	765
ρ (kg ·m^{-3})	997.1	3970
k (W·m^{-1}·k^{-1})	0.613	40
α(m^2·s)	1.47 × 10^7	131.7 × 10^7
β(K^{-1})	21 × 10^{-5}	0.85 × 10^{-5}

The continuity, momentum and energy equations which govern two-dimensional laminar free convection along with the Boussinesq approximation are as follows

$$\frac{\partial u}{\partial x}+\frac{\partial v}{\partial y}=0 \tag{1}$$

$$u\frac{\partial u}{\partial x}+v\frac{\partial u}{\partial y}=-\frac{1}{\rho_{nf}}\frac{\partial p}{\partial x}+\frac{\mu_f}{\rho_f}\left(\frac{\partial^2 u}{\partial x^2}+\frac{\partial^2 u}{\partial y^2}\right) \tag{2}$$

$$u\frac{\partial u}{\partial x}+v\frac{\partial u}{\partial y}=-\frac{1}{\rho_{nf}}\frac{\partial p}{\partial y}+\frac{\mu_f}{\rho_f}\left(\frac{\partial^2 v}{\partial x^2}+\frac{\partial^2 v}{\partial y^2}\right)+\frac{(\rho\beta)_{nf}\partial y}{\rho_{nf}}g(T-T_c) \tag{3}$$

$$u\frac{\partial T}{\partial x}+v\frac{\partial T}{\partial y}=\alpha_{nf}\left(\frac{\partial^2 T}{\partial x^2}+\frac{\partial^2 T}{\partial y^2}\right) \tag{4}$$

where the effective density, thermal expansion coefficient, heat capacity and thermal diffusivity of the nanofluid are stated as follows

$$\rho_{nf}=(1-\varphi)\,\rho_f+\varphi\rho_s \tag{5}$$

$$(\rho\beta)_{nf}=(1-\varphi)\,(\rho\beta)_f+\varphi(\rho\beta)_s \tag{6}$$

$$(\rho c_p)_{nf}=(1-\varphi)(\rho c_p)_f+\varphi(\rho c_p)_s \tag{7}$$

$$\alpha_{nf}=\frac{k_{nf}}{(\rho c_p)_{nf}} \tag{8}$$

Here φ is the volume fraction of nanoparticles.

The nanofluid effective thermal conductivity, k_{nf} is calculated using Maxwell equation [28].

$$\frac{k_{nf}}{k_f} = \frac{\left(k_s + 2k_f\right) - 2\varphi\left(k_f - k_s\right)}{\left(k_s + 2k_f\right) + \varphi\left(k_f - k_s\right)} \tag{9}$$

The use of this equation is restricted to spherical nanoparticles and this model is found to be appropriate for studying heat transfer enhancement using nanofluids [29,30].
The Brinkman model [31] is employed to estimate effective dynamic viscosity of nanofluid

$$\mu_{nf} = \frac{\mu_f}{(1-\varphi)^{2.5}} \tag{10}$$

The following dimensionless parameters are used to convert the governing equations to dimensionless form

$$X = \frac{x}{H}\,,\;\; Y = \frac{y}{H}\,,\;\; V = \frac{vH}{\alpha_f}\,,\;\; U = \frac{uH}{\alpha_f}\,,\;\; P = \frac{pH^2}{\rho_{nf}{\alpha_f}^2}\,,\;\; \theta = \frac{T - T_c}{T_h - T_c} \tag{11}$$

Thus the governing equations in non-dimensional form are stated as follows

$$\frac{\partial U}{\partial X} + \frac{\partial V}{\partial Y} = 0 \tag{12}$$

$$U\frac{\partial U}{\partial X} + V\frac{\partial U}{\partial Y} = -\frac{\partial P}{\partial X} + \frac{\nu_{nf}}{\alpha_f}\left(\frac{\partial^2 u}{\partial x^2} + \frac{\partial^2 u}{\partial y^2}\right) \tag{13}$$

$$U\frac{\partial U}{\partial X} + V\frac{\partial V}{\partial Y} = -\frac{\partial P}{\partial Y} + \frac{\nu_{nf}}{\alpha_f}\left(\frac{\partial^2 V}{\partial X^2} + \frac{\partial^2 V}{\partial Y^2}\right) + \frac{(\rho\beta)_{nf}}{\rho_{nf}\beta_f} RaPr\theta \tag{14}$$

$$U\frac{\partial \theta}{\partial X} + V\frac{\partial \theta}{\partial Y} = \frac{\alpha_{nf}}{\alpha_f}\left(\frac{\partial^2 \theta}{\partial X^2} + \frac{\partial^2 \theta}{\partial Y^2}\right) \tag{15}$$

where the Rayleigh number, Prandtl number and kinematic viscosity are defined as follows

$$Ra = \frac{g\beta_f (T_h - T_c) H^3}{\alpha_f \nu_f} \tag{16}$$

$$Pr = \frac{\nu_f}{\alpha_f} \tag{17}$$

$$\nu_f = \frac{\mu_f}{\rho_f} \tag{18}$$

Assuming no slip, the boundary conditions for Eqs. (12) - (15) are

$$\left.\begin{array}{l} \text{on walls og, oa, ob: } U = V = 0, \theta = 1 \\ \text{on walls og, oa, ob: } U = V = 0, \theta = 1 \\ \text{on walls cd, de, ef: } U = V = 0, \theta = 0 \\ \text{on walls bc, fg: } U = V = 0, \partial\theta/\partial n = 0 \end{array}\right\} \tag{19}$$

Where *n* denotes normal direction to the wall.

The local Nusselt number and average Nusselt number can be expressed as

$$Nu_{local} = -\frac{k_f}{k_f}\frac{\partial\theta}{\partial X} \text{ on wall oa} \tag{20}$$

$$Nu_{local} = -\frac{k_f}{k_f}\frac{\partial\theta}{\partial Y} \text{ on wall og and ab} \tag{21}$$

$$Nu = \frac{1}{3}\left(\int_0^1 Nu_{local}dX \mid_{Y=0} + \int_0^1 Nu_{local}dY \mid_{X=0} + \int_0^1 Nu_{local}dX \mid_{Y=1}\right) \tag{22}$$

3. Numerical Procedure and Validation

The governing equations are discretized using finite volume method and the diffusion terms in the equations are discretized by a second order differential equation. Coupling between pressure and velocity fields is committed using SIMPLER algorithm. A grid independence check has been performed on the C-shaped enclosure at AR = 0.4, $Ra = 10^6$, $\varphi = 0.1$ and without pins under variable number of mesh elements and the outcomes are presented in Table 2. From the results it is observed that the there is no significant changes in average Nusselt number for the mesh elements in between 32832 and 131328. Hence, the mesh with 32832 elements has been chosen to conduct the numerical analysis. In order to validate the numerical approach, a C-shaped enclosure filled with Cu nanoparticles has been considered and the average Nusselt number at AR = 0.4, $\varphi = 0.1$ for $Ra = 10^3$ and $Ra = 10^6$ have been compared with the reported data [14] as shown in Table 3.

Table 2. Grid independence check on the C-shaped enclosure at AR = 0.4, $Ra=10^6$, φ = 0.1 and without pins.

Mesh Elements	513	2052	8208	32832	131328
Nu	2.827	3.675	4.256	4.501	4.503

Table 3. Comparison of the average Nusselt number between Cu-water nanofluid filled C-shaped enclosure at φ= 0.1, AR = 0.4 and the reported data [14]

Rayleigh Number	Mahmoodi Simulation	Present Simulation	|Error| (%)
$Ra=10^3$	*Nu*=1.206	*Nu*=1.237	2.57
$Ra=10^6$	*Nu*=4.564	*Nu*=4.501	1.38

4. Results and Discussion

To investigate the heat transfer performance of C-shaped enclosures filled with Al_2O_3-water nanofluid temperature, velocity and total heat flux profiles are generated for two different Rayleigh numbers and volume fractions of the nanoparticles. The consequence of inserting four cylindrical pins has also been studied. The results discussed here are

based on fixed aspect ratio (AR) 0.4, Rayleigh numbers 10^3 and 10^6 and volume fraction 0 and 0.1.

The streamlines and the isotherms for AR = 0.4 and φ = 0 for different Rayleigh numbers are presented in Figs. 2 and 4 respectively and those for φ = 0.1 are presented in Figs. 3 and 5 respectively. From the streamlines at $Ra = 10^3$, it is observed that the fluid is initially heated by the hot walls and moves upward by the cause of thermal expansion. Then the cooling and compression of fluid takes place in the cold rib. Eventually, the compressed fluid moves downward generating a clockwise eddy in the whole portion of the enclosure. Formation of a counter clockwise secondary eddy takes place at higher Rayleigh number $Ra = 10^6$ in the space between bottom hot wall and cold rib. The clockwise and counter clockwise eddies have been represented by negative and positive values respectively as shown in streamlines distribution. Because of higher strength of primary eddy at $Ra = 10^6$, the primary eddy is strong enough to penetrate the region between upper hot wall and cold rib.

An even distribution of the isotherms at $Ra = 10^3$ are observed inside the enclosure demonstrating heat transfer dominated by conduction. At $Ra = 10^6$, formation of distinct thermal boundary layers close to all isothermal walls except the top wall takes place. Shifting of dominant heat transfer mechanism from conduction to free convection occurs at $Ra = 10^6$ due to disturbance in isotherms. Nanoparticles being added to pure water, fluid properties like viscosity and thermal conductivity are enhanced. At $Ra = 10^3$ the effect of addition Al_2O_3 is not prominent. But at $Ra = 10^6$ streamlines and isotherms become smother and evenly spaced demonstrating improved flow and temperature profiles. Because of higher viscosity of nanofluid, primary eddy becomes stronger to suppress the formation of secondary eddy to a little extent.

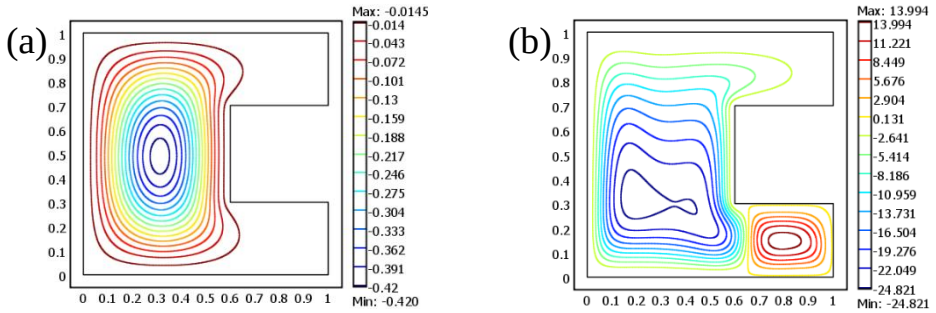

Fig. 2. Streamlines inside the enclosure with AR = 0.4 and for pure fluid, (a) $Ra = 10^3$, (b) $Ra = 10^6$.

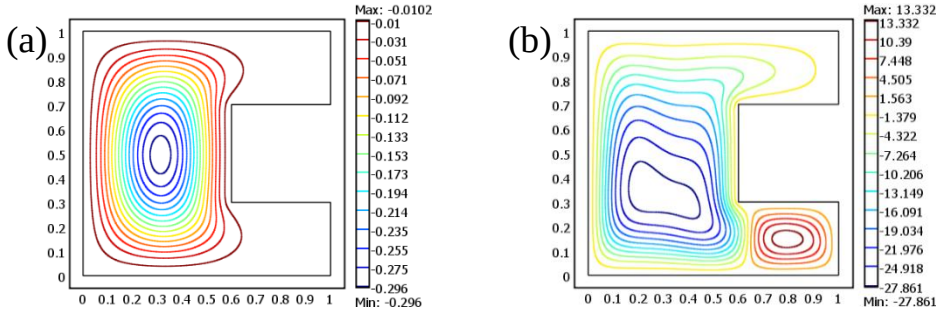

Fig. 3. Streamlines inside the enclosure with AR = 0.4 and for φ= 0.1, (a) $Ra = 10^3$, (b) $Ra = 10^6$.

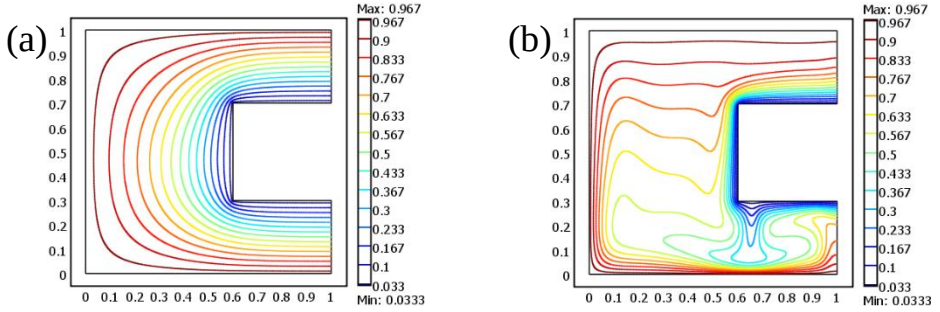

Fig. 4. Isotherms inside the enclosure with AR = 0.4 and for pure fluid, (a) $Ra = 10^3$, (b) $Ra = 10^6$.

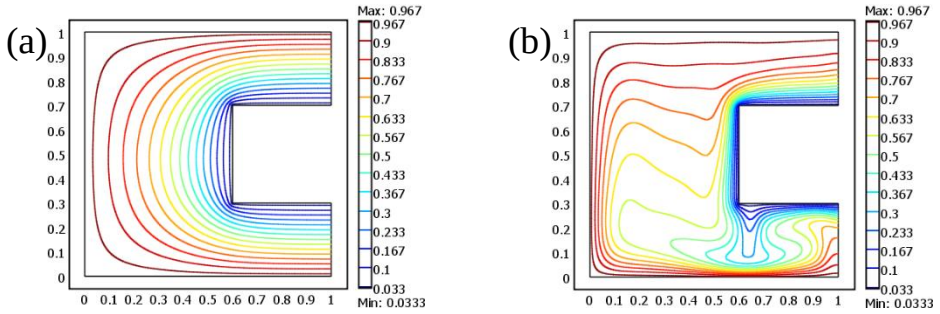

Fig. 5. Isotherms inside the enclosure with AR = 0.4 and for φ= 0.1, (a) $Ra = 10^3$, (b) $Ra = 10^6$.

Total heat flux profiles for pure fluid and nanofluid have been shown in Figs. 6 and 7 respectively. Maximum heat flux of pure fluid at $Ra = 10^6$ is found to be about fifteen times of maximum heat flux at $Ra = 10^3$ due to increased fluid motion. Due to addition of 10 % nanoparticles, effective heat transfer surface area increases followed by reduction in total heat flux in both cases at $Ra = 10^3$ and $Ra = 10^6$. Therefore, with the depletion of

heat flux, the possibility of boiling crisis i.e., departure from nucleate boiling (DNB) and critical heat flux (CHF) is also reduced.

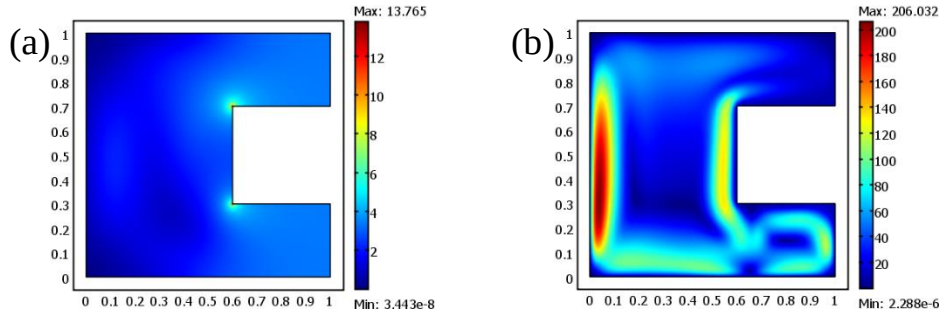

Fig. 6. Total heat flux of pure fluid with AR = 0.4, (a) $Ra = 10^3$, (b) $Ra = 10^6$.

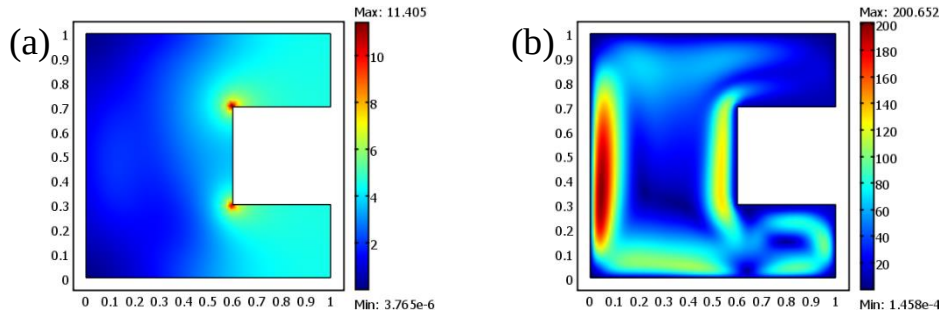

Fig. 7. Total heat flux of nanofluid with AR = 0.4, $\varphi = 0.1$, (a) $Ra = 10^3$, (b) $Ra = 10^6$.

Modified Schematic diagrams of the C-shaped enclosure under consideration with AR = 0.4 and inserted pins have been shown in Fig. 8. Four pins have been inserted throughout the length of the enclosure. Figs. 9-14 shows the streamlines, isotherms and heat flux profiles for R/H = 0.05, while Figs. 15-20 represent those for $R/H = 0.08$. Here R denotes the radius of the cylindrical pins.

Figs. 15, 17 and 19 represent the streamlines, isotherms and total heat flux distribution respectively of pure fluid with AR = 0.4 and having 4 pins of $R/H = 0.05$. Streamlines are found to be obstructed by the cylindrical pins. Though at $Ra = 10^3$ formation of only primary eddy is observed, generation of comparatively weaker secondary eddy takes place at $Ra = 10^6$ due to disturbance in the fluid. Moreover, insertion of pins have lowered the penetrating tendency of primary eddy at $Ra = 10^6$ in the region between upper hot wall and cold rib. The presence of pins has caused isotherms to approach each other particularly near the pin walls. As heat transfer is dominated by conduction at $Ra = 10^3$, isotherms are found to be evenly distributed. On the other hand at $Ra = 10^6$, formation of distinct thermal boundary layers close to all isothermal walls except the top wall takes place indicating free convection dominated heat transfer mechanism. Additionally,

cylindrical pins have increased the effective heat transfer area and hence total heat flux is decreased to a little extent.

Figs. 16, 18 and 20 show the streamlines, isotherms and total heat flux distribution respectively of nanofluid (φ = 0.1) with AR = 0.4 and having 4 pins of *R/H* = 0.05. The effect of nanoparticles addition is hardly observed at $Ra = 10^3$. But at $Ra = 10^6$ formation of secondary eddy is curtailed, isotherms become smoother as well as heat flux is reduced on availability of more effective heat transfer area.

The streamlines, isotherms and total heat flux distribution of pure fluid with AR = 0.4 and having 4 pins of *R/H*= 0.08 have been displayed in Figs. 15, 17 and 19 respectively. Due to bigger radii of pins, streamlines are more disturbed generating secondary eddies at $Ra = 10^6$. The tendency of the isotherms to approach towards the pin walls also increases along with the increase in pin size. Total heat flux of fluid behaves contrastively for different Rayleigh numbers. Heat flux of fluid at $Ra = 10^6$ has increased due to serious obstruction from larger pins resulting reduced effective heat transfer area. The streamlines, isotherms and total heat flux distribution of nanofluid (φ = 0.1) with AR = 0.4 and having 4 pins of *R/H* = 0.08 have been shown in Figs. 16, 18 and 20 respectively. At $Ra = 10^6$ formation of secondary eddy is suppressed to a great extent and isotherms are observed to be smoother. Addition of nanoparticles has boosted the heat flux at $Ra = 10^3$ but lowered the heat flux at $Ra = 10^6$ due to enormous disturbance created by pins and nanoparticles together in heat transfer mechanism.

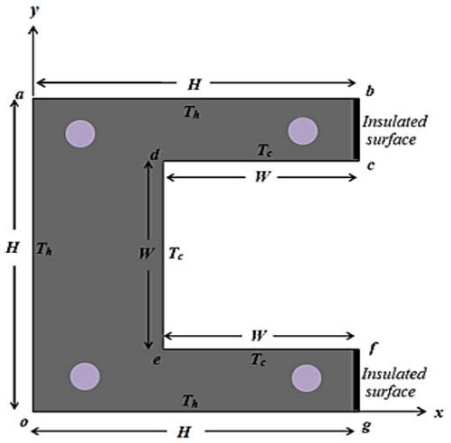

Fig. 8. Modified Schematic diagram of the C-shaped enclosure under consideration with 4 cylindrical pins.

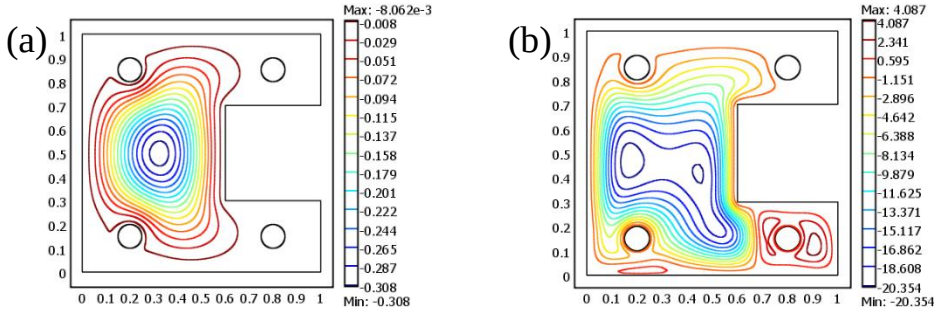

Fig. 9. Streamlines inside the enclosure with AR = 0.4, having 4 pins of R/H = 0.05 and pure fluid, (a) $Ra = 10^3$, (b) $Ra = 10^6$.

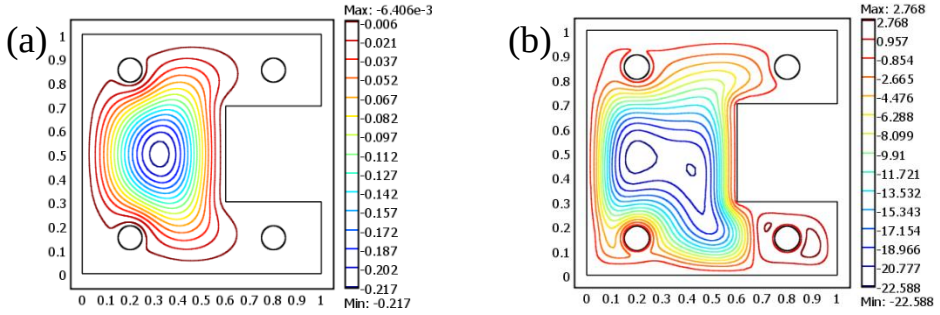

Fig. 10. Streamlines inside the enclosure with AR = 0.4, having 4 pins of R/H = 0.05, φ= 0.1, (a) $Ra = 10^3$, (b) $Ra = 10^6$.

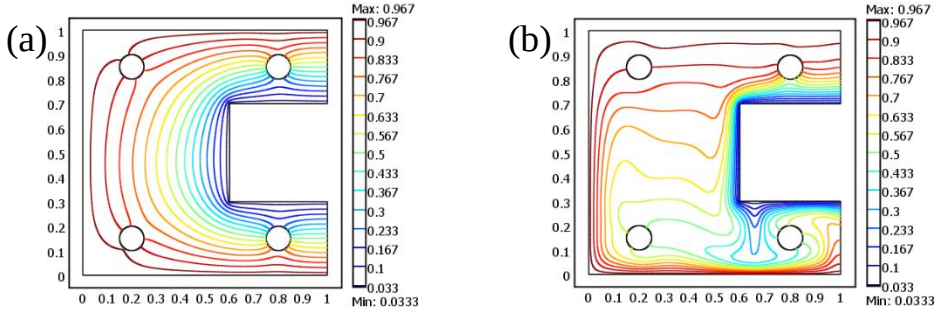

Fig. 11. Isotherms inside the enclosure with AR = 0.4, having 4 pins of R/H = 0.05 and for pure fluid, (a) $Ra = 10^3$, (b) $Ra = 10^6$.

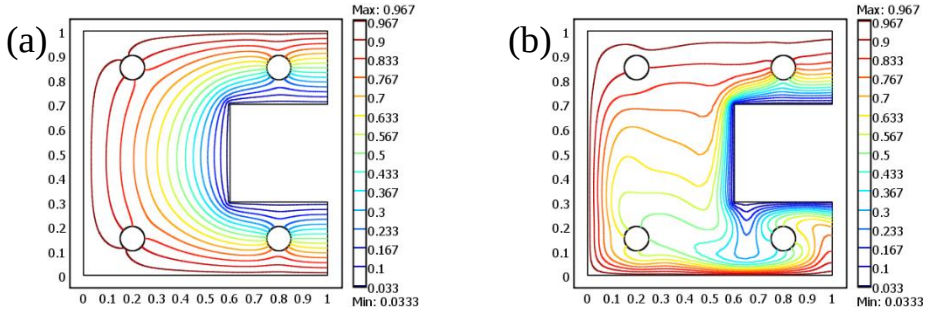

Fig. 12. Isotherms inside the enclosure with AR = 0.4, having 4 pins of R/H = 0.05 and for φ= 0.1, (a) $Ra = 10^3$, (b) $Ra = 10^6$.

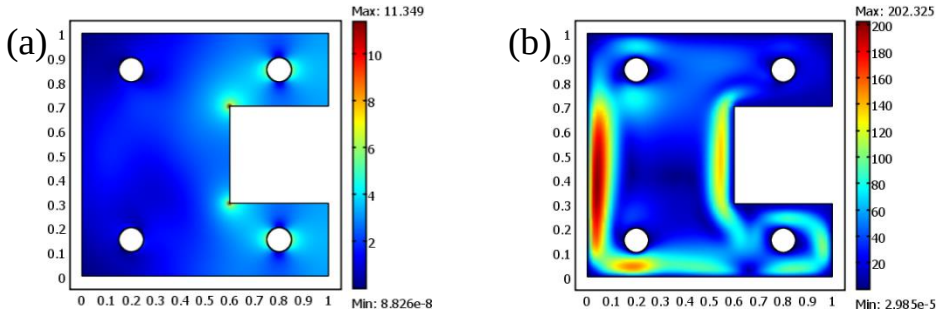

Fig. 13. Total heat flux of pure fluid with AR = 0.4 and having 4 pins of R/H = 0.05, (a) $Ra = 10^3$, (b) $Ra = 10^6$.

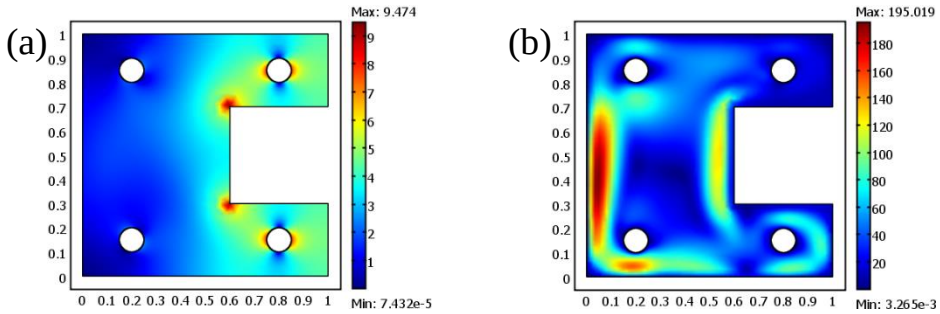

Fig. 14. Total heat flux of nanofluid with AR = 0.4, having 4 pins of R/H = 0.05 and φ= 0.1, (a) $Ra = 10^3$, (b) $Ra = 10^6$.

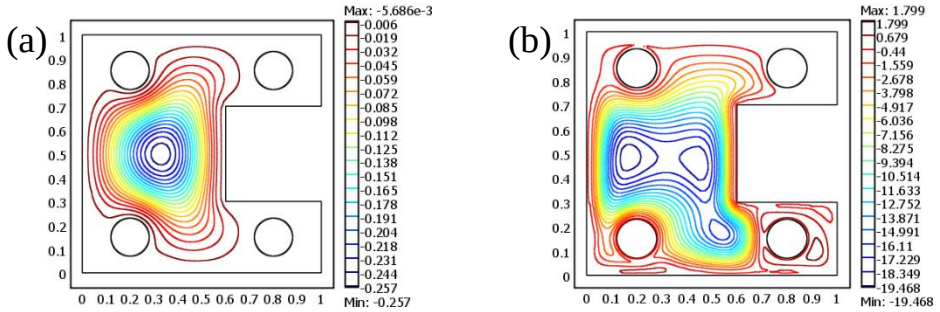

Fig. 15. Streamlines inside the enclosure with AR = 0.4, having 4 pins of *R/H* = 0.08 and pure fluid, (a) $Ra = 10^3$, (b) $Ra = 10^6$.

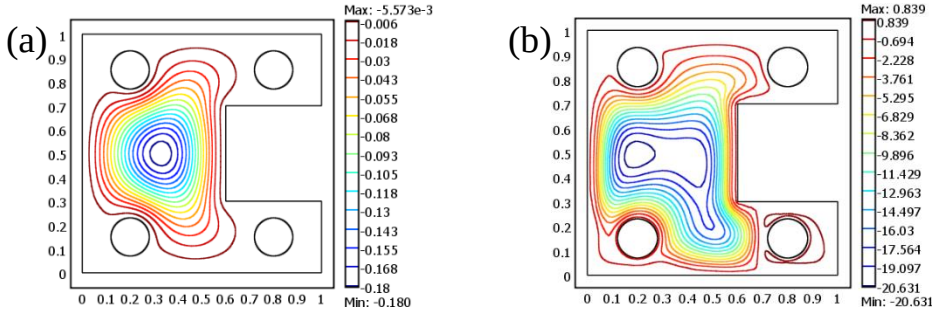

Fig. 16. Streamlines inside the enclosure with AR = 0.4, having 4 pins of *R/H* = 0.08 and φ= 0.1, (a) $Ra = 10^3$, (b) $Ra = 10^6$.

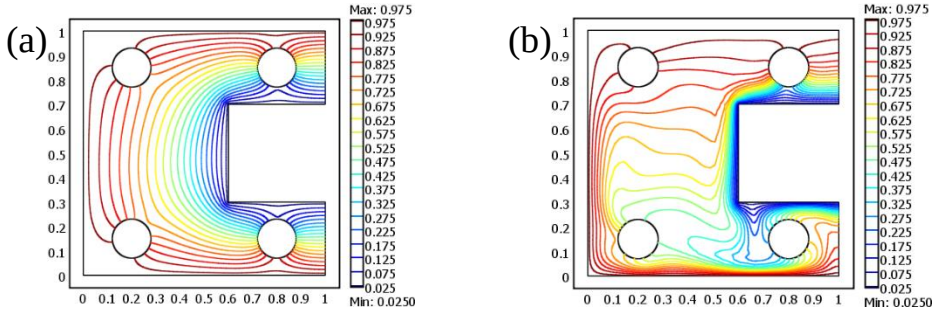

Fig. 17. Isotherms inside the enclosure with AR = 0.4, having 4 pins of *R/H* = 0.08 and pure fluid, (a) $Ra = 10^3$, (b) $Ra = 10^6$.

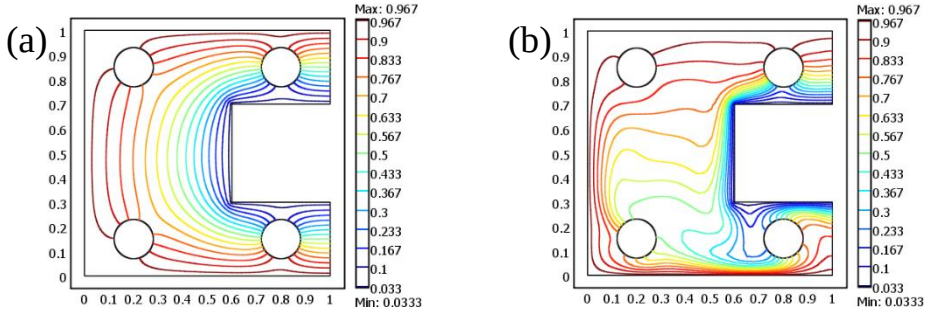

Fig. 18. Isotherms inside the enclosure with AR = 0.4, having 4 pins of R/H = 0.08 and φ= 0.1, (a) $Ra = 10^3$, (b) $Ra = 10^6$.

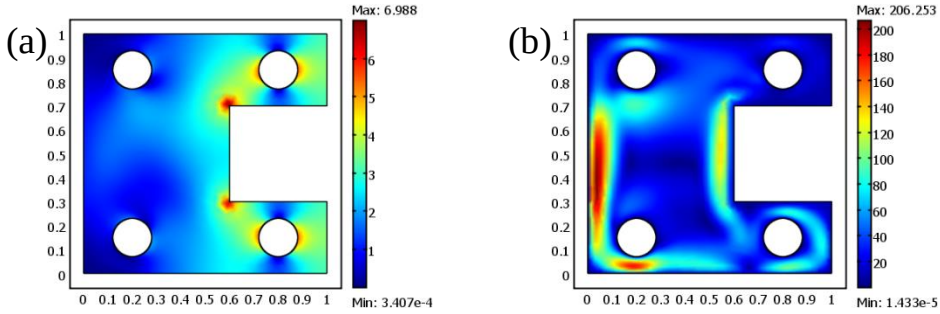

Fig. 19. Total heat flux of pure fluid with AR = 0.4 and having 4 pins of R/H = 0.08 (a) $Ra = 10^3$, (b) $Ra = 10^6$.

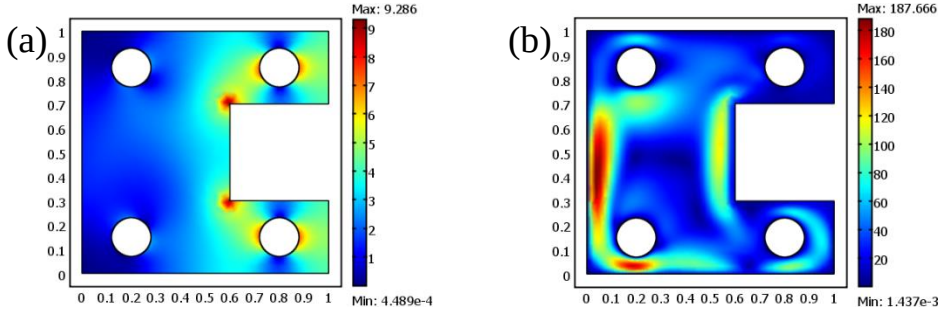

Fig. 20. Total heat flux of nanofluid with AR = 0.4, having 4 pins of R/H = 0.08 and φ = 0.1, (a) $Ra = 10^3$, (b) $Ra = 10^6$

Fig. 21 demonstrates the variation of average Nusselt number with variable Rayleigh number and nanoparticles volume fraction. From the graphs, it is obvious that average Nusselt number increases with increasing Rayleigh number. In absence of cylindrical pins, average Nusselt number increases with the addition of 10 % nanoparticles. Pins with R/H = 0.05 enhances the Nusselt number both in pure fluid and nanofluid at both Rayleigh

numbers considered. Hence, heat transfer rate as well as the overall efficiency of the cooling system is improved. On the other hand, pins with *R/H* = 0.08 creates much disturbance in the pure fluid at $Ra = 10^6$ and in the nanofluid at $Ra = 10^3$. Therefore, the average Nusselt number is observed to be lower than the expected value.

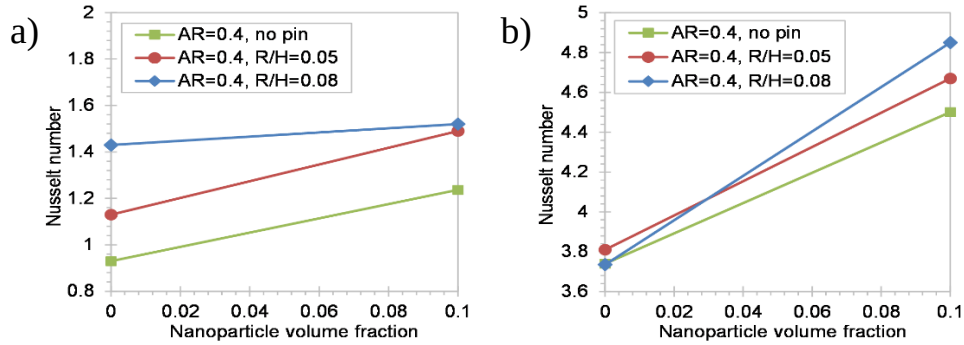

Fig. 21. Variation of average Nusselt number with nanoparticles volume fraction at AR=0.4, (a) $Ra = 10^3$, (b) $Ra = 10^6$.

5. Conclusion

In this paper, the effect of volume fraction of nanoparticles, Rayleigh number and radii of cylindrical pins on temperature, velocity and total heat flux profile have been studied numerically using finite volume method for C-shaped enclosures filled with Al_2O_3-water nanofluid. For AR = 0.4, $Ra = 10^6$ secondary eddies are developed in the region between bottom hot wall and cold rib of enclosure under consideration. Therefore, at higher Rayleigh number the heat transfer mechanism is governed by free convection. 10% alumina nanoparticles being added to pure water viscosity, thermal conductivity and effective heat transfer area of the fluid are enhanced significantly. As a result, streamlines and isotherms become more smother and evenly spaced, thereby improving the heat transfer performance. Addition of 10 % nanoparticle and insertion of cylindrical pins of *R/H* = 0.05 increases the effective heat transfer area to a considerable amount. Hence, total heat flux is decreased while average Nusselt number is increased. On the other hand, pins with *R/H* = 0.08 create immense disturbance in nanofluid reducing the average Nusselt number at $Ra = 10^3$ while increasing at $Ra = 10^6$. Therefore, pins of optimum radius are suggested for C-shaped enclosure. Insertion of cylindrical pins weakens the secondary eddy formation and forces the isotherms to approach to each other particularly near the pin walls.

6. Nomenclature

AR	aspect ratio of enclosure
C_p	specific heat, $J \cdot kg^{-1} \cdot K^{-1}$
g	acceleration due to gravity, $m \cdot s^{-2}$

h	heat transfer co-efficient, $W \cdot m^{-2} \cdot K^{-1}$
k	thermal conductivity, $W \cdot m^{-1} \cdot K^{-1}$
H	enclosure height, m
W	enclosure thickness, m
R	cylindrical pin radius, m
Nu	Nusselt number
p	pressure, $N \cdot m^{-2}$
P	dimensionless pressure
Pr	Prandtl number
q	heat flux, $W \cdot m^{-2}$
Ra	Rayleigh number
T	Dimensional temperature, K
u,v	dimensional velocities components in x and y direction, $m \cdot s^{-1}$
U,V	dimensionless velocities components in X and Y direction
x,y	dimensional Cartesian co-ordinates, m
X,Y	dimensionless Cartesian co-ordinates

Greek symbols

α	thermal diffusivity, $m^2 \cdot s$
β	thermal expansion co-efficient, K^{-1}
θ	dimensionless temperature
μ	dynamic viscosity, $kg \cdot m^{-1} \cdot s$
ν	kinematic viscosity, $m^2 \cdot s^{-1}$
ρ	density, $kg \cdot m^{-3}$
φ	nanoparticle volume fraction

Subscripts

c	cold
f	fluid
h	hot
s	solid particles

References

1. S. Ostrach, Adv. Heat Transf. **8**, 161 (1972). https://doi.org/10.1016/S0065-2717(08)70039-X
2. C. J. Ho, M. W. Chen, and Z. W. Li, Int. J. Heat Mass Tran. **51**, 4506 (2008). https://doi.org/10.1016/j.ijheatmasstransfer.2007.12.019
3. O. Abouali and A. Falahatpisheh, Heat Mass Transfer **46**, 15 (2009). https://doi.org/10.1007/s00231-009-0540-7
4. M. Shahi, A. H. Mahmoudi, and F.Talebi, Int. Commun. Heat Mass **37**, 1535 (2010). https://doi.org/10.1016/j.icheatmasstransfer.2010.08.005
5. F. H. Lai and Y. T. Yang, Int. J. Therm. Sci. **50**, 1930 (2011). https://doi.org/10.1016/j.ijthermalsci.2011.04.015
6. M. F. Asad, M. M. A. Sarker, and M. J. H. Munshi, J. Sci. Res. **11**, 173 (2019). https://doi.org/10.3329/jsr.v11i2.38797
7. H. F. Oztop and E. Abu-Nada, Int. J. Heat Fluid Flow **29**, 1326 (2008). https://doi.org/10.1016/j.ijheatfluidflow.2008.04.009
8. E. Abu-nada and H. F. Oztop, Int. J. Heat Fluid Flow **30**, 669 (2009). https://doi.org/10.1016/j.ijheatfluidflow.2009.02.001

9. E. Abu-nada, Z. Masoud, H. F. Oztop and A. Campo, Int. J. Therm. Sci. **49**, 479 (2010). https://doi.org/10.1016/j.ijthermalsci.2009.09.002
10. E. B. Ögüt, Int. J. Therm. Sci. **48**, 2063 (2009). https://doi.org/10.1016/j.ijthermalsci.2009.03.014
11. B. Ghasemi and S. M. Aminossadati, Int. J. Therm. Sci. **49**, 931 (2010). https://doi.org/10.1016/j.ijthermalsci.2009.12.017
12. G. A. Sheikhzadeh, A. Arefmanesh, and M. Mahmoodi, J. Nano Res. **13**, 75 (2011). https://doi.org/10.4028/www.scientific.net/JNanoR.13.75
13. M. Mahmoodi, Int. J. Therm. Sci. **50**, 1731 (2011). https://doi.org/10.1016/j.ijthermalsci.2011.04.009
14. M. Mahmoodi and S. M. Hashemi, Int. J. Therm. Sci. **55**, 76 (2012). https://doi.org/10.1016/j.ijthermalsci.2012.01.002
15. M. Mansour, M. Bakeir, and A.Chamkha, Int. J. Numer. Method Heat Fluid Flow **24**, 1954 (2014). https://doi.org/10.1108/HFF-06-2013-0198
16. N. Makulati, A. Kasaeipoor, and M. M. Rashidi, Adv. Powder Technol. **27**, 661 (2016). https://doi.org/10.1016/j.apt.2016.02.020
17. A. J. Chamkha, M. A. Ismael, A. Kasaeipoor, and T. Armaghani, Entropy **18**, 50 (2016). https://doi.org/10.3390/e18020050
18. R. Mohebbi, M. Izadi, and A. J. Chamkha, Phys. Fluids **29**, ID 122009 (2017) https://doi.org/10.1063/1.4993866
19. S. Kumar and A. Kumar, Int. J. Ambient Energy (2018). https://doi.org/10.1080/01430750.2018.1530139
20. M. Sheikholeslami, M. Gorji-Bandpy, and D. D. Ganji, Energy **60**, 501 (2013). http://dx.doi.org/10.1016/j.energy.2013.07.070
21. H. E. Ahmed, M. I. Ahmed, and M. Z. Yusoff, Appl. Therm. Eng. **91**, 191 (2015). https://doi.org/10.1016/j.applthermaleng.2015.07.061
22. G. K. Sinha and A. Srivastava, Int. J. Heat Mass Tran. **108**, 1140 (2017). https://doi.org/10.1016/j.ijheatmasstransfer.2016.12.085
23. M. A. Sheremet, I. Pop, and O. Mahian, Int. J. Heat Mass Trans. **116**, 751 (2018). https://doi.org/10.1016/j.ijheatmasstransfer.2017.09.070
24. G. Wang, Y. Zhang, J. Zhang, and B. Ma, Chem. Eng. Trans. **61**, 1171 (2017) https://doi.org/10.3303/CET1761193
25. D. D. Vo, M. Hedayat, T. Ambreen, S. A. Shehzad, M. Sheikholeslami, A. Shafee, and T. K. Nguyen, J. Therm. Anal. Calorim. **139**, 1345 (2020). https://doi.org/10.1007/s10973-019-08501-4
26. H. F. Oztop, E. Abu-Nada, Y. Varol, and K. Al-Salem, Superlattice Microst. **49**, 453 (2011). https://doi.org/10.1016/j.spmi.2011.01.002
27. A. Bejan, Convection Heat Transfer. 4thEdition, (John Wiley & Sons, Inc., New Jersey, 2004).
28. J. A. Maxwell, A Treatise on Electricity and Magnetism, 2nd Edition (Oxford University Press, Cambridge, 1904).
29. A. Akbarinia and A. Behzadmehr, Appl. Therm. Eng. **27**, 1327 (2007). https://doi.org/10.1016/j.applthermaleng.2006.10.034
30. E. Abu-Nada, Int. J. Heat Fluid Flow **29**, 242 (2008). https://doi.org/10.1016/j.ijheatfluidflow.2007.07.001
31. H. C. Brinkman, J. Chem. Phys. **20**, 571 (1952). https://doi.org/10.1063/1.1700493